ACS APPLIED MATERIALS & INTERFACES

Research Article

www.acsami.org

High Strain in $(K,Na)NbO_3$ -Based Lead-Free Piezoceramics

Hong Tao,[†] Jiagang Wu,*[,†] Dingquan Xiao,[†] Jianguo Zhu,[†] Xiangjian Wang,[‡] and Xiaojie Lou[‡]

[†]Department of Materials Science, Sichuan University, Chengdu 610064, P. R. China

[‡]Multi-disciplinary Materials Research Center, Frontier Institute of Science and Technology, and State Key Laboratory for Mechanical Behavior of Materials, Xi'an Jiaotong University, Xi'an 710049, P. R. China

ABSTRACT: A high strain is important for practical applications of piezoelectric actuators. Here we reported a high strain in the $(K,Na)NbO_3$ -based ceramics by doping alkaline earths or transition metals. The ceramics possess a high strain (~0.29%) as well as a large converse piezoelectric coefficient ($d33^*$) up to 688 pm/V, which almost matches that of PZT4 ceramics. The obtained d_{33}* is high for nontextured $(K,Na)NbO_3$-based ceramics. In addition, a higher d_{33} value (340–407 pC/N) was also attained in the ceramics. Enhanced d_{33} and d_{33}* values of this work should be attributed to the multiphase coexistence's effect induced by alkaline earths or transition metals. We believe that our research can benefit the developments of $(K,Na)NbO_3$ ceramics and widen their applications range.

Material System	S_{max}/E_{max} (pm/V)	d_{33} (pC/N)	TC (oC)	Ref.
KNNS-BNKZ-ZZ	688	407	234	This work
KNN-$LiTaO_3$	150-310	150-240	310~445	12
$(K,Na,Li)(Nb,Ta,Sb)O_3$	750	416	253	3
BNT-BT-KNN	560	<100	T_d<200	11
$(Ba,Ca)(Ti,Zr)O_3$	1100~1200	620	90	4
PZT4	700	410	250	27

KEYWORDS: *lead-free piezoceramics, $(K,Na)NbO_3$, high strain*

INTRODUCTION

To protect our surviving environment, the lead-based piezoceramics will be finally replaced by the lead-free counterparts.[1,2] In the past ten years, the lead-free counterparts have endured an incredible development because of their excellent properties.[3−5] Among all investigated lead-free candidates, the alkali niobate ceramics have drawn great attention since Saito et al. realized a breakthrough in piezoelectric constant ($d_{33} \approx 416$ pC/N) of the textured $(K,Na,Li)(Nb,Ta,Sb)O_3$ ceramics,[3] and more recently a large d_{33} value (~490 pC/N) has been developed in the $(K,Na)NbO_3$ (KNN) -based lead-free ceramics.[5] According to the recent developments of lead-free piezoceramics,[1−3,5−12] it is no doubt that the KNN material can be considered to be one of the most promising candidates for replacing $Pb(Zr,Ti)O_3$.

In the past decades, an inferior piezoelectricity of KNN -based ceramics has restricted its progresses in replacing PZT.[1,2] Recently, there has been a big breakthrough in its piezoelectric activity, and a d_{33} value of ~490 pC/N has been realized in the KNN -based ceramics by constructing rhombohedral-tetragonal (R-T) phase boundary.[5] In addition, the electric field -induced strains of lead-free piezoceramics become a new highlight, exceeding those of lead-based ceramics.[3,13] As a result, lots of researchers have also paid great attention to the strain studies on lead-free materials.[3,13−16] For example, a giant strain of 0.45% was observed in the $(Bi,Na)TiO_3$−$BaTiO_3$-$(K,Na)NbO_3$ ternary systems,[13] whereas a poor d_{33} value is always shown. Recently, Bortolani F. et al. has developed the microfiber ceramics concerning the KNN -based piezoelectric fibers, and a high strain value of ~0.17% at 3 kV mm^{-1} results from an extrinsic effect.[16] Although the KNN -based ceramics possess good piezoelectric properties, a relatively low strain of <0.2% is also often demonstrated.[3,14,15] As a result, the unbalanced development of both d_{33} and strain is a confusing problem for most researchers. It may be wondered whether a large d_{33} and a high strain can be simultaneously attained in the same KNN ceramics. Previous studies show that a high strain of KNN -based ceramics can result from the instability of polarization vector induced by the multiphases transition regions.[17] As a result, we hope to realize both a large d_{33} and a high strain in the KNN-based ceramics by constructing multiphase transition region using the refining compositions.

In this work, the $0.96(K_{0.48}Na_{0.52})(Nb_{0.95}Sb_{0.05})O_3$-0.04[0.9 $Bi_{0.5}(Na_{0.18}K_{0.82})_{0.5}ZrO_3$ −0.1$AZrO_3$] (KNNS-BNKZ-AZ: A = Mg^{2+}, Zn^{2+}, Cu^{2+}, Ba^{2+}, Sr^{2+}, and Ca^{2+}) ceramics were prepared by the conventional solid-state method in order to simultaneously realize both a large d_{33} and a high strain. By choosing optimum alkaline earths and transition metals, the ceramics doped with Zn^{2+} simultaneously possess a large d_{33} (~407 pC/N) and a high strain (0.29%), realizing our established objective. In addition, there are few reports on such good comprehensive performance of d_{33} and strain in alkali niobate, and such a result also matches those of part PZT. The related physical mechanisms for enhanced electrical properties were also addressed.

EXPERIMENTAL SECTION

The KNNS-BNKZ-AZ ceramics were prepared by the solid state synthesis from the raw materials of K_2CO_3 (99%), Na_2CO_3 (99.8%), Nb_2O_5 (99.5%), Sb_2O_3 (99.99%), Bi_2O_3 (99.999%), ZrO_2 (99%), MgO (99%), ZnO (99%), CuO (99%), $BaCO_3$ (99%), $SrCO_3$ (99%), and $CaCO_3$ (99%). The weighed powders were mixed together with the ZrO_2 balls for 24 h in isopropanol, and then the calcinations were conducted at 850 °C for a dwell time of 6 h. Finally, the dried mixtures were added with 8 wt % poly(vinyl alcohol) (PVA) as a binder for

Received: August 30, 2014
Accepted: October 27, 2014
Published: November 11, 2014

granulation and then pressed into disks of ~10 mm in diameter and ~1.0 mm in thickness under a pressure of 10 MPa. All green pellets were sintered at 1065−1110 °C in air after removing the PVA. The Ag electrodes were covered onto both parallel surfaces for characterizing their electrical properties. The samples were subsequently poled at 30 °C under an applied electric field of ~40 kV/cm for a dwell time of 30 min. The surface morphologies of each sample were examined by the field emission-scanning electron microscopy (FE-SEM, JSM-7500, Japan), and the element mapping of Zn -modified ceramics was conducted by the energy-dispersive spectrometry (EDS) of FE-SEM. The relative molar ratios of the elements in the samples doped with Zn were determined using the X-ray photo electron spectroscopy (XPS, Kratos AXIS Ultra DLD, Japan). The phase purity and crystal structure of the samples were analyzed by the X-ray diffraction (XRD) machine with a PANalytical X'Pert PRO X-ray diffractometer with a CuK_α radiation (λ = 1.54187 Å) operating at 40 kV and 40 mA. The relative permittivity and dielectric loss of the samples were measured using an *LCR* meter (HP 4980, Agilent, U.S.A.) in the unpoled state. Temperature dependence of the dielectric properties of the unpoled samples was conducted upon heating from −150 to 450 °C at 1 °C/min, at a frequency of 100 kHz. The d_{33} values of the poled samples were characterized by a quasi-static d_{33} meter (ZJ-3A, IACAS, China). Their polarization against electric field (*P*−*E*) hysteresis loops were conducted using a standardized ferroelectric test system at room temperature. The strains that developed under the applied electric fields at 10 Hz and room temperature were measured with a MTI-2000 fotonic sensor.

RESULTS AND DISCUSSION

Here the effects of alkaline earth (e.g., Mg^{2+}, Ba^{2+}, Sr^{2+}, and Ca^{2+}) and transition metals (e.g., Zn^{2+} and Cu^{2+}) on the phase structure of the ceramics were studied by analyzing their XRD patterns and temperature-dependent dielectric constant (ε_r vs *T*) curves. Figure 1a displays the effects of different ions

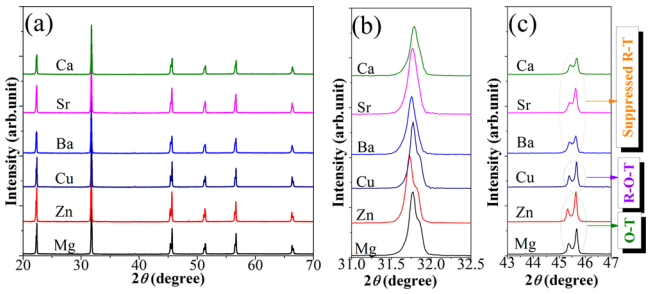

Figure 1. XRD patterns of the ceramics with Mg^{2+}, Zn^{2+}, Cu^{2+}, Ba^{2+}, Sr^{2+}, and Ca^{2+}, measured at (a) 2θ = 20−70°, (b) 2θ = 31−32.5°, and (c) 2θ = 43−47°.

on the XRD patterns of the ceramics, measured at 2θ = 20−70°. In the investigated compositions range, all the ceramics show a pure perovskite phase, showing the formation of a stable solid solution. To further clarify the difference in the XRD diffraction peaks, the correspondingly amplified XRD patterns are given in Figure 1b, c. We can see the obvious differences in the XRD shapes in the 2θ range of 31−32.5°, that is, the double peaks emerge when the ions substitutions change from Mg^{2+}, Zn^{2+}, Cu^{2+} to Ba^{2+}, Sr^{2+}, Ca^{2+} (see Figure 1b). In addition, the XRD diffraction peaks located at 2θ = 43−47° gradually draw close when the types of ion substitutions change from Mg^{2+}, Zn^{2+}, Cu^{2+} to Ba^{2+}, Sr^{2+}, Ca^{2+}, as shown in Figure 1c. Those results strongly show that their phase transitions happen when alkaline earths or transition metals were used in these ceramics. The ε_r vs *T* curves could be used to well evaluate the phase transitions of KNN -based ceramics.[5,6] In this work, we measured the ε_r vs *T* curves of the ceramics as a function of alkaline earths and transition metals (see Figure 2), characterized at *f* = 100 kHz and −150−200 °C. For Mg^{2+}, Zn^{2+}, or Cu^{2+} modifications, two permittivity peaks were shown (see Figure 2a−c), which are assigned to the corresponding $T_{R\text{-}O}$ and $T_{O\text{-}T}$, respectively. As shown in Figure 2a, b, $T_{R\text{-}O}$ is below room temperature for the ones with Mg^{2+} or Zn^{2+}, whereas $T_{O\text{-}T}$ is almost close to room temperature, showing that such two ceramics possess the O-T phase coexistence at room temperature.[6] However, there is a different trend for the Cu^{2+} -doped ceramics, that is, both $T_{R\text{-}O}$ and $T_{O\text{-}T}$ are close room temperature (see Figure 2c), confirming that the mixed phases concerning R, O, and T were involved at room temperature. Moreover, we can observe that the R-T phase boundary is suppressed in the ceramics doped with Ba^{2+}, Sr^{2+}, or Ca^{2+}, where their dielectric peaks for ε_r vs *T* curves become much more broadened, as shown in Figure 2d−f. As a result, the phase structure of the ceramics has been clearly identified, as listed below: O-T for Mg^{2+} and Zn^{2+}, R-O-T for Cu^{2+}, and suppressed R-T for Ba^{2+}, Sr^{2+}, and Ca^{2+}.

To study the influences of alkaline earths and transition metals on their T_C and dielectric loss (tan δ), the curves of dielectric properties (i.e., ε_r and tan δ) against *T* were measured at 50−450 °C and *f* = 100 kHz, as plotted in Figure 3(a). All ceramics possess similar ε_r vs *T* curves, and one dielectric peak was only observed, corresponding to its T_C. In addition, we can also observe from Figure 3a that similar tan δ vs *T* curves ware shown in all the ceramics, which are slightly dependent on the doped alkaline earths and transition metals. We gave the T_C, $T_{O\text{-}T}$, and $T_{R\text{-}O}$ values of the ceramics, where all data was collected from Figures 2 and 3a, as shown in Figure 3b. The Mg^{2+} or Zn^{2+} -doped ceramics possess a higher T_C value than those of the ones with Cu^{2+}, Ba^{2+}, Sr^{2+}, or Ca^{2+}. Previously, the doping with optimum Zn^{2+} or Mg^{2+} content can increase T_C of KNN,[18,19] and the doping with Zn^{2+} or Mg^{2+} induces the increase of T_C of this work. Unfortunately, the ions (e.g., Cu^{2+}, Ba^{2+}, Sr^{2+}, or Ca^{2+}) result in the decrease of T_C in the ceramics.[19−22] In addition, their phase structure evolutions have been clarified using the phase diagrams established by considering XRD patterns as well as ε_r vs *T* curves shows, as plotted in Figure 3b. For the Mg^{2+}, Zn^{2+}, or Cu^{2+}-modified ceramics, $T_{O\text{-}T}$ increases as the doping elements change from Mg^{2+} and Zn^{2+} to Cu^{2+}. It was reported that the addition of Mg^{2+} leads to the decrease of $T_{O\text{-}T}$ in KNN,[19] whereas $T_{O\text{-}T}$ will be increased by adding Zn^{2+} or Cu^{2+}.[18,20] In addition, the Cu^{2+} can more quickly promote $T_{O\text{-}T}$ of KNN than that of Zn^{2+}.[18,20] The $T_{R\text{-}O}$ of the ceramics could be raised by doping Mg^{2+}, Zn^{2+}, or Cu^{2+}, while its R-T phase boundary was suppressed by doping Ba^{2+}, Sr^{2+}, or Ca^{2+}, where the ε_r vs *T* curves become more broadened.[19,22,23] Such a phenomenon is mainly ascribed to the decreased grain sizes, as will be shown later.

Figure 4a−f shows the FE-SEM images of the ceramics with alkaline earths and transition metals. The different grain growth modes were observed in those ceramics, which are dependent on the types of doping elements. The ceramics doped with Mg^{2+}, Zn^{2+}, or Cu^{2+} possess a bimodal grain size distribution, whereas uniform and smaller grain sizes were observed in the ones modified with Ba^{2+}, Sr^{2+}, or Ca^{2+}. It was reported that the doping with Zn^{2+}, Cu^{2+} or Mg^{2+} easily induces the abnormal grain growths of KNN -based ceramics.[18,20,24] However, the grain sizes of KNN -based ceramics were decreased by doping Ba^{2+}, Sr^{2+} or Ca^{2+}. Usually, the doping with Ba^{2+} inhibits the

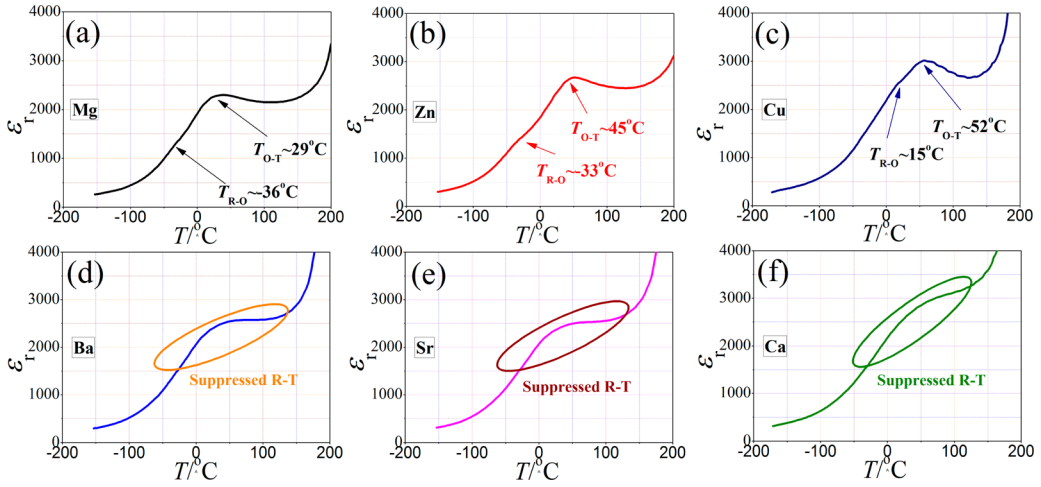

Figure 2. ε_r vs T of the ceramics doped with (a) Mg^{2+}, (b) Zn^{2+}, (c) Cu^{2+}, (d) Ba^{2+}, (e) Sr^{2+}, and (f) Ca^{2+}, measured at −150−200 °C and 100 kHz.

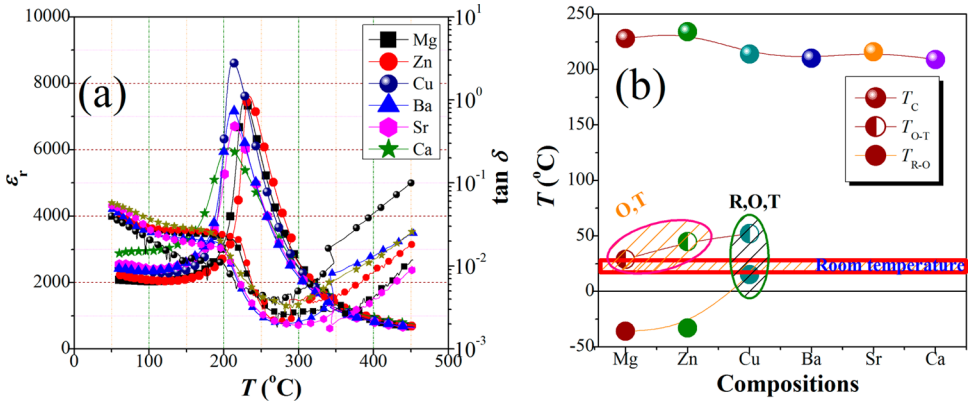

Figure 3. (a) ε_r and tan δ vs T (50−450 °C) of the ceramics doped with Mg^{2+}, Zn^{2+}, Cu^{2+}, Ba^{2+}, Sr^{2+}, and Ca^{2+}. (b) Phase diagram of the ceramics.

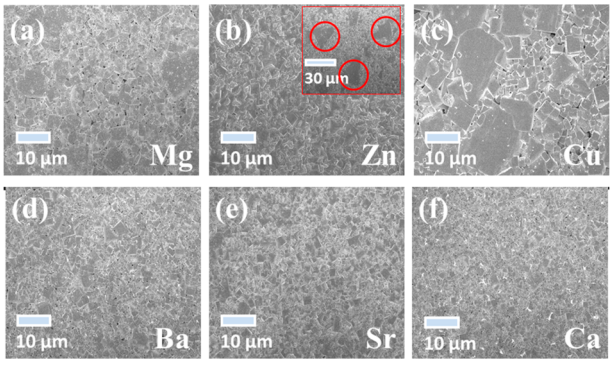

Figure 4. SEM images of the ceramics doped with (a) Mg^{2+}, (b) Zn^{2+}, (c) Cu^{2+}, (d) Ba^{2+}, (e) Sr^{2+}, and (f) Ca^{2+}.

grain growths of KNN ceramics because that Ba^{2+} easily locates at the grain boundaries and slows down their mobility,[22] weakening the transportation and resulting in the decreased grain sizes. The doping with Sr^{2+}[23] or Ca^{2+} induces the grains inhabitation, as the Ba^{2+} does.[22] To further show the morphologies evolution (e.g., grain size), we characterized the grain size distributions of the ceramics, as shown in Figure 5. The ceramics with Ba^{2+}, Sr^{2+}, or Ca^{2+} possess a narrow grain size distribution, and a wider grain size distribution is shown in the ones with Mg^{2+}, Zn^{2+}, or Cu^{2+} (see Figure 5a−f). That is, the grain size distribution shifts toward larger grain sizes and becomes much broader when the Mg^{2+}, Zn^{2+}, or Cu^{2+} was used. As shown in the inset of Figure 5a, the ceramics with Mg^{2+}, Zn^{2+}, or Cu^{2+} possess a larger average grain size with respect to the ones with Ba^{2+}, Sr^{2+}, or Ca^{2+}.

To clearly show the homogeneously compositional distributions and identify the existence of the elements, we characterized the element mapping and the composition analysis of the Zn-doped ceramics, respectively. We can observe from Figure 6 that all the elements are homogeneously distributed in the whole ceramic matrix. However, it was found that the Zn cannot be detected by EDS because of the limitation of accuracy and a low Zn content. To confirm the existence of all the elements, the XPS analysis for all involved elements was conducted, as shown in the inset of Figure 6 as well as Figure 7. The collected data indicates that the K, Na, Nb, Sb, Bi, Zn, Zr, and O of the ceramics are involved. Table 1 gives the composition analysis of the ceramics characterized by XPS and EDS. We can see that the compositions characterized by XPS and EDS are different from its theoretical values because of the detection limitations of these machines, the involvement of light elements, and the loss of alkali metals. In addition, previous reports also show that it is difficult to accurately characterize the compositions of KNN-based ceramics because of too many involved elements including light elements.[25] However, we can also derive some useful information from Table 1 that the Na^+ in KNN more easily evaporates than that of K^+ during sintering, which matches these reported results in KNN-based ceramics.[25]

Figure 8a plots the ferroelectric properties of the ceramics with Mg^{2+}, Zn^{2+}, Cu^{2+}, Ba^{2+}, Sr^{2+}, and Ca^{2+}, characterized at

dx.doi.org/10.1021/am505887y | ACS Appl. Mater. Interfaces 2014, 6, 20358−20364

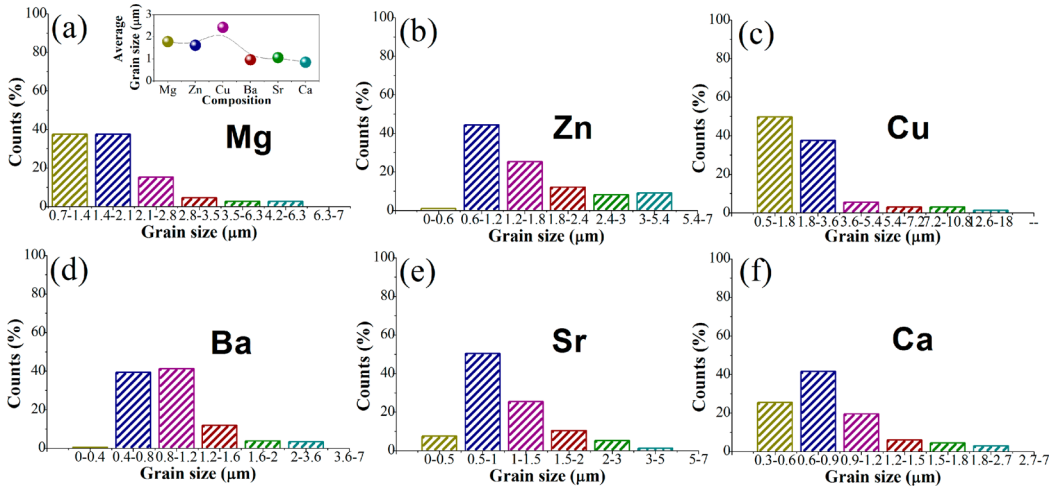

Figure 5. Grain size distribution of the ceramics doped with (a) Mg^{2+}, (b) Zn^{2+}, (c) Cu^{2+}, (d) Ba^{2+}, (e) Sr^{2+}, and (f) Ca^{2+}, where all data were derived from Figure 4. The inset in a is the composition dependence of average grain size.

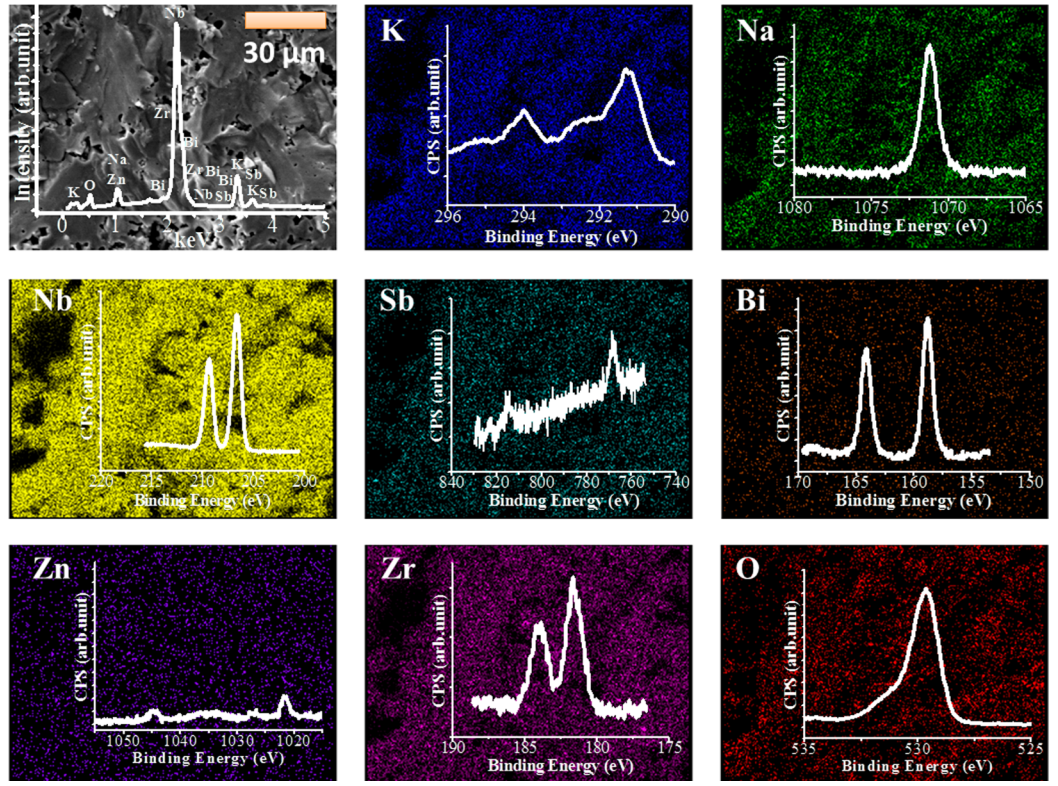

Figure 6. Elements (K, Na, Nb, Sb, Bi, Zn, Zr, and O) mapping of cross-section in the ceramics doped with Zn^{2+}, and the inset is their corresponding XPS profile.

Table 1. Composition Analysis of the Ceramics Doped with Zn by XPS and EDS

	K	Na	Nb	Sb	Bi	Zn	Zr	O
theoretical value	9.51	10.05	18.24	0.96	0.36	0.08	0.80	60.00
EDS	10.02	8.48	29.50	1.00	1.33	0.00	0.59	49.08
XPS	7.05	3.61	16.66	1.52	0.43	0.30	0.66	69.77

room temperature and f = 10 Hz. Their P–E loops are strongly dependent on the types of the additives, and more saturated P–E loops were observed in the Mg^{2+}, Zn^{2+}, or Cu^{2+}-modified ceramics as compared with the ones doped with Ba^{2+}, Sr^{2+}, or Ca^{2+}. It was found that optimum Cu^{2+}, Zn^{2+}, or Mg^{2+} content should induce a typical "square" ferroelectric hysteresis loop,[24,26] whereas the addition of Ba^{2+}, Sr^{2+}, or Ca^{2+} always weakens the ferroelectric properties of KNN-based ceramics.[22] Their P_r and E_c values derived from P–E loops were shown in the inset of Figure 8a in order to characterize their ferroelectric properties evolution. A larger P_r value was observed in the ceramics with the additives of Mg^{2+}, Zn^{2+}, or Cu^{2+},[18,26−28]

dx.doi.org/10.1021/am505887y | ACS Appl. Mater. Interfaces 2014, 6, 20358−20364

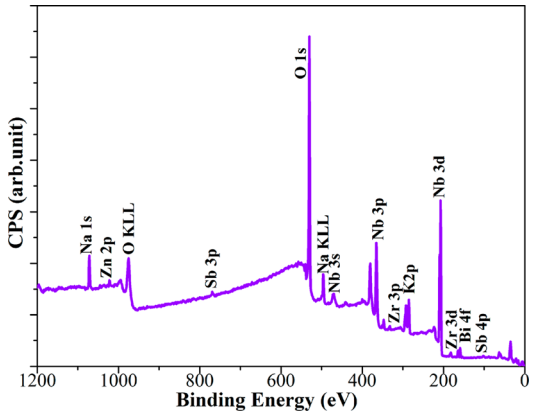

Figure 7. XPS profiles of the cross-section in the ceramics doped with Zn^{2+}.

whereas there is a slight change in their E_c value. In addition, the ceramics with Ba^{2+},[22] Sr^{2+},[29] or Ca^{2+}[30] exhibit the degraded ferroelectric properties and unsaturated $P-E$ loops.[19] Figure 8b shows the dielectric constant (ε_r) and dielectric loss (tan δ) of the ceramics with different additives. The doping with Mg^{2+}, Zn^{2+}, or Cu^{2+} decreases the tan δ of the ceramics, while a high tan δ value was shown in the Ba^{2+}, Sr^{2+}, or Ca^{2+}-modified ceramics.[24] However, the different trends were observed in the ε_r vs. compositions, and a higher ε_r value is shown in Cu^{2+}-modified ceramics.

Figure 9 plots the d_{33} and k_p of the ceramics doped with Mg^{2+}, Zn^{2+}, Cu^{2+}, Ba^{2+}, Sr^{2+}, and Ca^{2+}. A similar trend is shown in both d_{33} and k_p, that is, the ceramics with Mg^{2+}, Zn^{2+} or Cu^{2+} have higher d_{33} and k_p than those of the ones with Ba^{2+}, Sr^{2+}, or Ca^{2+}. In this work, a large d_{33} value of >300 pC/N was attained in the ceramics doped with Mg^{2+}, Zn^{2+} or Cu^{2+}, whereas the doping with Ba^{2+}, Sr^{2+}, or Ca^{2+} deteriorates d_{33} of 100−250 pC/N. First, the types of phase boundaries are mainly responsible for the difference in their d_{33}. Second, the lattice distortions also strongly affect their piezoelectric activity besides the types of the phase boundaries, that is, a smaller lattice distortion can benefit the improvement in d_{33} of KNN -based ceramics.[31] Recent researches have shown that the second poling process can benefit the improved piezoelectricity of KNN -based ceramics.[7] In this work, we polarized each sample after the thermal process (processing temperatures > T_C), and their d_{33} value is listed in Figure 10a. It shows that the second poling process can greatly improve the piezoelectricity of all ceramics. For example, the d_{33} value of the Zn^{2+} -doped ceramics increases from 331 pC/N to 407 pC/N after the second poling process. The second-poling method induces the enhanced piezoelectric properties owing to the migration of oxygen vacancies as well as the interaction between defect dipoles and spontaneous polarization inside domains.[7] Thermal stability is also an important parameter for the practical applications of a piezoelectric material. Figure 10b shows the thermal stability of d_{33} of the ceramics after the second poling process. A better thermal stability of d_{33} was observed in the ceramics with Mg^{2+}, Zn^{2+}, or Cu^{2+} as compared with the ones with Ba^{2+}, Sr^{2+} or Ca^{2+}. In addition, we also gave the aging behavior of piezoelectric constant in the Zn -modified ceramics, as shown in the inset of Figure 10b. It was found that the ceramics possess good aging behavior of the piezoelectricity, that is, the d_{33} value almost keeps unchanged after 26 weeks.

In the field of electric field -induced strains, considerable attention has been given to lead-free ceramics, especially BNK-BKT-KNN.[13] Although this BNK-BKT-KNN material system possesses a large strain, there is a poor d_{33} value.[13] On the contrary, the KNN-based ceramics have a large d_{33} as well as a poor strain. In this work, the electric field -induced strain of the

Table 2. Compared Analysis of Strain, d_{33}, and T_C

material systen	S_{max}/E_{max} (pm/V)	d_{33} (pC/N)	T_C (°C)	ref
KNNS-BNKZ-ZZ	688	407	234	this work
KNN-$LiTaO_3$	150−310	150−240	310−445	12
$(K,Na,Li)(Nb,Ta,Sb)O_3$	750	416	253	3
BNT-BT-KNN	560	<100	T_d < 200	11
$(Ba,Ca)(Ti,Zr)O_3$	1100−1200	620	90	4
PZT4	700	410	250	27

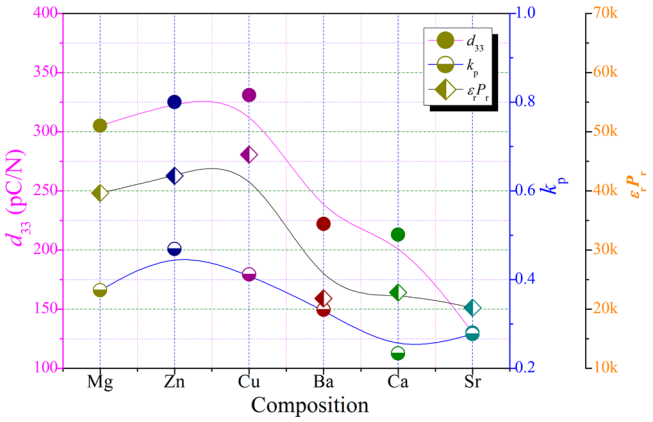

Figure 9. d_{33} and k_p as well as $\varepsilon_r P_r$ of the ceramics doped with Mg^{2+}, Zn^{2+}, Cu^{2+}, Ba^{2+}, Sr^{2+}, and Ca^{2+}.

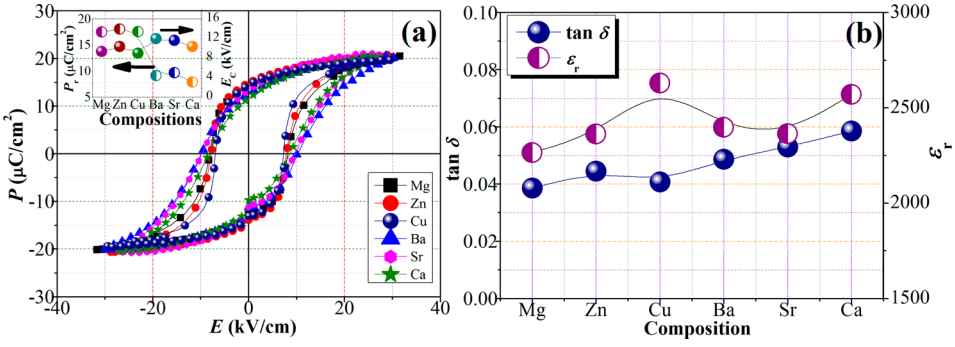

Figure 8. (a) $P-E$ loops and (b) ε_r and tan δ of the ceramics doped with Mg^{2+}, Zn^{2+}, Cu^{2+}, Ba^{2+}, Sr^{2+}, and Ca^{2+}. The inset is P_r and E_C against composition.

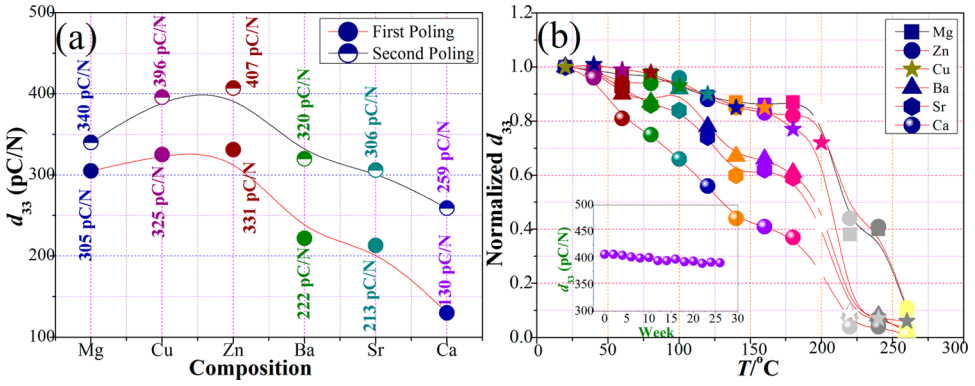

Figure 10. d_{33} of the ceramics doped with Mg^{2+}, Zn^{2+}, Cu^{2+}, Ba^{2+}, Sr^{2+}, and Ca^{2+} after first and second poling process. (b) Thermal stability of d_{33} of the ceramics doped with Mg^{2+}, Zn^{2+}, Cu^{2+}, Ba^{2+}, Sr^{2+}, and Ca^{2+} after the second poling process, and the inset is aging behavior of the ceramics doped with Zn^{2+}.

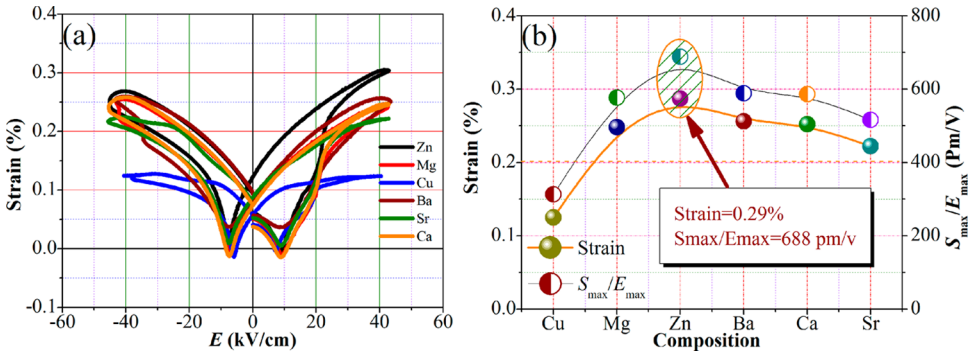

Figure 11. (a) Electric field-induced strain curves as well as (b) strain and S_{max}/E_{max} of the ceramics doped with Mg^{2+}, Zn^{2+}, Cu^{2+}, Ba^{2+}, Sr^{2+}, and Ca^{2+}.

ceramics was conducted and shown in Figure 11a, measured at f = 10 Hz and room temperature. All ceramics possess a typical strain curve with a butterfly shape. In addition, the strain and d_{33}* (d_{33}* = S_{max}/E_{max}) of the ceramics are shown in Figure 11b. The strain value first increases and then drops, reaching a relatively high value (~0.29%) for the ceramics doped with Zn^{2+}. In addition, the d_{33}* gradually increases and then dramatically decreases with the changed compositions, getting a maximum value of ~688 pm/V. Such a high strain value of 0.29% (~688 pm/V) is much larger than previously reported results in KNN-based ceramics.[3,14,15] As a result, large d_{33} and high strain have been simultaneously realized in the Zn^{2+} -doped ceramics. In addition, a large d_{33} value was also observed in such a ceramic, as shown in Table 2. As a result, the comprehensive performance of strain and d_{33} is superior to those of $Bi_{1/2}Na_{1/2}TiO_3$ and other KNN-based ceramics (see Table 2), and is comparable to those of PZT4 and textured $(K,Na,Li)(Nb,Ta,Sb)O_3$ ceramics. Although both strain and d_{33} are slightly inferior to that of $(Ba,Ca)(Ti,Zr)O_3$, the ceramics of this work possesses a higher T_C, which can widen application temperature range. As a result, this material system possesses a good comprehensive performance of strain (S_{max}/E_{max} ≈ 688 pm/V), d_{33} (~407 pC/N), and T_C (~234 °C).

CONCLUSION

We attained a high electric field-induced strain in the $(K,Na)NbO_3$-based ceramics by the addition of alkaline earth and transition metals (e.g., Mg^{2+}, Ba^{2+}, Sr^{2+}, Ca^{2+}, Zn^{2+}, and Cu^{2+}), and also investigated the evolutions of phase structure and electrical properties. The phase boundaries will be altered by doping different additives of Mg^{2+}, Zn^{2+}, Cu^{2+}, Ba^{2+}, Sr^{2+}, or Ca^{2+}, and their T_C and microstructure were also affected by those additives. A large electric field -induced strain (~0.22−0.29%) was observed in all ceramics except for Cu^{2+}, and the corresponding S_{max}/E_{max} (516−688 pm/v) was also shown. It is of great interest to note that a large d_{33} and a high strain were simultaneously attained in the same material system, which is superior to currently reported results in other lead-free materials (e.g., BNT and KNN). As a result, alkaline earth and transition metals well tailor the piezoelectricity and strain of KNN-based material systems.

AUTHOR INFORMATION

Corresponding Author

*E-mail: msewujg@scu.edu.cn or wujiagang0208@163.com.

Notes

The authors declare no competing financial interest.

ACKNOWLEDGMENTS

Authors gratefully acknowledge the supports of the National Science Foundation of China (NSFC 51272164, 51332003, and 51472169), and the Fundamental Research Funds for the Central Universities (2012SCU04A01), and the College of Materials Science and Engineering of Sichuan University. We thank Ms. Hui Wang for measuring the SEM patterns.

REFERENCES

(1) Shrout, T. R.; Zhang, S. Lead-free Piezoceramics: Alternatives for PZT? *J. Electroceram* **2007**, *19*, 111−124.

(2) Rödel, J.; Jo, W.; Seifert, K.; Anton, E. M.; Granzow, T.; Damjanovic, D. Perspective on the Development of Lead-free Piezoceramics. *J. Am. Ceram. Soc.* **2009**, *89*, 1153−1177.
(3) Saito, Y.; Takao, H.; Tani, T.; Nonoyama, T.; Takatori, K.; Homma, T.; Nagaya, T.; Nakamura, M. Lead-free Piezoceramics. *Nature* **2004**, *432*, 84−87.
(4) Liu, W.; Ren, X. Large Piezoelectric Effect in Pb-Free Ceramics. *Phys. Rev. Lett.* **2009**, *103*, 257602.
(5) Wang, X. P.; Wu, J. G.; Xiao, D. Q.; Zhu, J. G.; Cheng, X. J.; Zheng, T.; Zhang, B. Y.; Lou, X. J.; Wang, X. J. Giant Piezoelectricity in Potassium-Sodium Niobate Lead-free Ceramics. *J. Am. Chem. Soc.* **2014**, *136*, 2905−2910.
(6) Guo, Y.; Kakimoto, K.; Ohsato, H. Phase Transitional Behavior and Piezolectric Properties of $(Na_{0.5}K_{0.5})NbO_3$-$LiNbO_3$ Ceramics. *Appl. Phys. Lett.* **2004**, *85*, 4121−4123.
(7) Wang, K.; Li, J. F. Domain engineering of lead-Free Li-modified $(K,Na)NbO_3$ polycrystals with highly enhanced piezoelectricity. *Adv. Funct. Mater.* **2010**, *20* (12), 1924−1929.
(8) Akdoğan, E. K.; Kerman, K.; Abazari, M.; Safari, A. Origin of High Piezoelectric Activity in Ferroelectric $(K_{0.44}Na_{0.52}Li_{0.04})$-$(Nb_{0.84}Ta_{0.1}Sb_{0.06})O_3$ Ceramics. *Appl. Phys. Lett.* **2008**, *92*, 112908.
(9) Matsubara, M.; Yamaguchi, T.; Sakamoto, W.; Kikuta, K.; Yogo, T.; Hirano, S. Processing and Piezoelectric Properties of Lead-Free $(K,Na)(Nb,Ta)O_3$ Ceramics. *J. Am. Ceram. Soc.* **2005**, *88* (5), 1190−1196.
(10) Cheng, X.; Wu, J.; Lou, X.; Wang, X.; Wang, X.; Xiao, D.; Zhu, J. Achieving Both Giant d_{33} and High T_C in Patassium-Sodium Niobate Ternary System. *ACS Appl. Mater. Interfaces* **2014**, *6* (2), 750−756.
(11) Rubio-Marcos, F.; Ochoa, P.; Fernandez, J. F. Sintering and properties of lead-free $(K,Na,Li)(Nb,Ta,Sb)O_3$ ceramics. *J. Eur. Ceram. Soc.* **2007**, *27* (13−15), 4125−4129.
(12) Rubio-Marcos, F.; Campo, A. D.; López-Juárez, R.; Romero, J. J.; Fernández, J. F. High spatial resolution structure of $(K,Na)NbO_3$ lead-free ferroelectric domains. *J. Mater. Chem.* **2012**, *22*, 9714−9720.
(13) Zhang, S. T.; Kounga, A. B.; Aulbach, E.; Ehrenberg, H.; Rödel, J. Giant Strain in Lead-Free Piezoceramics $Bi_{0.5}Na_{0.5}TiO_3$−$BaTiO_3$−$K_{0.5}Na_{0.5}NbO_3$ System. *Appl. Phys. Lett.* **2007**, *91* (11), 112906.
(14) Hollenstein, E.; Davis, M.; Damjanovic, D.; Setter, N. Piezoelectric Properties of Li-and Ta-modified $(K_{0.5}Na_{0.5})NbO_3$ Ceramics. *Appl. Phys. Lett.* **2005**, *87*, 182905.
(15) Wang, K.; Li, J. F.; Zhou, J. J. High Normalized Strain Obtained in Li-Modified $(K,Na)NbO_3$ Lead-Free Piezoceramics. *Appl. Phys. Express* **2011**, *4*, 061501.
(16) Bortolani, F.; Campo, A.; Fernandez, J. F.; Clemens, F.; Rubio-Marcos, F. High Strain in $(K,Na)NbO_3$-Based Lead-Free Piezoelectric Fibers. *Chem. Mater.* **2014**, *26* (12), 3838−3848.
(17) Yan, K.; Ren, X. Multi-phase transition behaviour and large electrostrain in lead-free (K, Na, Li)NbO_3 ceramics. *J. Phys. D: Appl. Phys.* **2014**, *47*, 015309.
(18) Rubio-Marcos, F.; Romero, J. J.; Navarro-Rojero, M. G.; Fernandez, J. F. Effect of ZnO on the structure, microstructure and electrical properties of KNN-modified piezoceramics. *J. Eur. Ceram. Soc.* **2009**, *29* (14), 3045−3052.
(19) Chang, Y. F.; Yang, Z.; Wei, L.; Liu, B. Effects of $AETiO_3$ additions on phase structure, microstructure and electrical properties of $(K_{0.5}Na_{0.5})NbO_3$ ceramics. *Mater. Sci. Eng., A* **2006**, *437*, 301−305.
(20) Rubio-Marcos, F.; Reinosa, J. J.; Vendrell, X.; Romero, J. J.; Mestres, L.; Leret, P.; Fernandez, J. F.; Marchet, P. Structure, microstructure and electrical properties of Cu^{2+} doped (K,Na,Li)-$(Nb,Ta,Sb)O_3$ piezoelectric ceramics. *Ceram. Int.* **2013**, *39*, 4139−4149.
(21) Lin, D. M.; Kwok, K. W.; Chan, H. L. W. Piezoelectric and ferroelectric properties of Cu-doped $K_{0.5}Na_{0.5}NbO_3$ lead-free ceramics. *J. Phys. D: Appl. Phys.* **2008**, *41*, 045401.
(22) Lin, D.; Kwok, K. W.; Chan, H. L. W. Effects of BaO on the structure and electrical properties of $0.95K_{0.5}Na_{0.5}(Nb_{0.94}Sb_{0.06})O_3$−$0.05LiTaO_3$ lead-free ceramics. *J. Phys. D: Appl. Phys.* **2007**, *40*, 6778−6783.
(23) Zheng, L. M.; Wang, J. F.; Ming, B. Q.; Qi, P.; Du, J. Phase Transition and High Piezoactivity of Sr Doped Lead-Free $(Na_{0.53}K_{0.422}Li_{0.048})$ $(Nb_{0.89}Sb_{0.06}Ta_{0.05})O_3$ Ceramics. *Chin. Phys. Lett.* **2008**, *25*, 2573−2576.
(24) Malic, B.; Bernard, J.; Holc, J.; Jenko, D.; Kosec, M. Alkaline-Earth Doping in $(K,Na)NbO_3$ Based Piezoceramics. *J. Eur. Ceram. Soc.* **2005**, *25* (12), 2707−2711.
(25) Cheng, L.; Wang, K.; Yao, F. Z.; Zhu, F.; Li, J. F. Composition Inhomogeneity due to Alkaline Volatilization in Li-Modified (K,Na)-NbO_3 Lead-Free Piezoceramics. *J. Am. Ceram. Soc.* **2013**, *96* (9), 2693−2695.
(26) Tan, X.; Fan, H.; Ke, S.; Zhou, L.; Mai, Y.; Huang, H. Structural dependence of piezoelectric, dielectric and ferroelectric properties of $K_{0.5}Na_{0.5}(Nb_{1-2x/5}Cu_x)O_3$ lead-free ceramics with high Q_m. *Mater. Res. Bull.* **2012**, *47*, 4472−4477.
(27) Park, S.; Ahn, C. W.; Nahm, S.; Song, J. Microstructure and Piezoelectric Properties of ZnO-added $(Na_{0.5}K_{0.5})NbO_3$ Ceramics. *Jpn. J. Appl. Phys.* **2004**, *43*, L1072−L1074.
(28) Li, E.; Kakemoto, H.; Wada, S.; Tsurumi, T. Influence of CuO on the Structure and Piezoelectric Properties of the Alkaline Niobate-Based Lead-Free Ceramics. *J. Am. Ceram. Soc.* **2007**, *90* (6), 1787−1791.
(29) Chen, Q.; Xu, Z.; Chu, R.; Hao, J.; Zhang, Y.; Li, G.; Yin, Q. Ferroelectric and dielectric properties of $Sr_{2-x}(Na, K)_xBi_4Ti_5O_{18}$ lead-free piezoelectric. *ceramics Phys. B* **2010**, *405*, 2781−2784.
(30) Taub, J.; Ramajo, L.; Castro, M. S. Phase structure and piezoelectric properties of Ca- and Ba-doped $K_{1/2}Na_{1/2}NbO_3$ lead-free ceramics. *Ceram. Int.* **2013**, *39*, 3555−3561.
(31) Sung, Y. S. Roles of Li and Ta in Pb-free piezoelectric $(Na,K)NbO_3$ ceramics. *Appl. Phys. Lett.* **2014**, *105*, 142903.